



Green synthesis of graphene acetic acid: A highly effective and versatile carbocatalyst for advanced oxidation reactions

Biagio Di Vizio^a, Giorgio Lazzari^a, Roman Strzelczyk^b, Giacomo De Crescenzo^a, Antonio Barbon^a, Claudio Garino^c, Roberto Gobetto^c, Stefano Agnoli^{a,d,*}

^a Department of Chemical Science and INSTM Unit, University of Padova, Via F. Marzolo 1, 35131, Padova, Italy

^b Institute of Molecular Physics, Polish Academy of Sciences, Smoluchowski Str. 17, 60-179, Poznan, Poland

^c Department of Chemistry and NIS Centre, University of Turin, Via Pietro Giuria 7, 10125, Torino, Italy

^d Consorzio Interuniversitario Reattività Chimica e Catalisi-CIRCC, Research Unit at the University of Padova, Via F. Marzolo 1, 35131, Padova, Italy

ABSTRACT

A novel graphene derivative with a high density (10 % at/at) of acetic acid pendants installed directly on the basal plane, called graphene acetic acid (GAA), is prepared through a sustainable protocol starting from fluorinated graphite. The proposed synthesis route is environmentally friendly, simple and highly scalable. The catalytic activity of the GAA as a peroxidase mimic is tested using standard protocols (i.e. 3,3',5,5'-tetramethylbenzidine (TMB) reacted with H₂O₂) obtaining excellent results that surpass the state of the art in previously reported carbon materials. To confirm further the versatility of GAA as an oxidation catalyst, and its potential relevance in industrial processes, we investigate the conversion of sulfides to sulfoxides. Once again, GAA proves to be an outstanding catalyst, being able to oxidize thioanisole to the corresponding sulfoxide in a short time (200 min for complete conversion) without the addition of a solvent and at room temperature. Moreover, the catalyst is easily recovered through filtration and can be subjected to further catalytic cycles without decreasing the performance.

1. Introduction

Since its discovery [1], graphene, a two-dimensional carbon allotrope [2], has attracted an increasing amount of interest from the scientific community. Initially studied primarily for its physical properties [3], later it has been intensively investigated for its catalytic activity [4–7]. In fact, despite being chemically inert in its pure stoichiometric form, defective or functionalized graphene exhibits an extremely diversified chemistry [8]. A variety of methodologies was developed to introduce into graphene specific functional groups or heteroatoms, for example high-temperature treatments [9], which however usually exhibit a poor control over sample morphology and functionalization selectivity, or fine synthesis protocols such as those based on fluorinated graphite (FG) [10]. In the latter case, different graphene materials with tailored functionalization [11,12] can be obtained through simple nucleophilic substitution reactions, taking advantage of the simultaneous radical defluorination responsible for restoring carbon sp² domains [13]. This synthetic strategy has been exploited to produce the so-called graphene acid [11], i.e. a monolayer graphenic nanosheet highly functionalized by carboxyl groups, which has proven to be an excellent catalyst [14] and a versatile platform for further functionalization [15]. This material is unique in that, despite being an oxidized

form of carbon similar to graphene oxide, it retains a remarkably high conductivity, making it an excellent redox mediator. Moreover, differently from standard graphene oxide, the carboxyl groups are installed not only on the sheet edges, but also directly on the basal plane. However, the use of potassium cyanide, a very dangerous and highly toxic compound, during the synthesis represents a major drawback for the practical application of this material. These considerations prompted us to find a synthesis strategy that could lead to a material with the same exceptional properties of graphene acid, but reduced environmental impact, and risk to human health [16].

Although the use of FG may raise concerns from a Green Chemistry standpoint, several relatively safe methods for its production exist, including photochemical and hydrothermal fluorination [17]. Moreover, the research on the subject is rapidly advancing [10], even exploring the potential for valorizing fluorinated polymer waste [18]. Lastly, one of the major limitations in the large-scale production of materials like graphene oxide is the poor reproducibility of their final properties [19], a problem that is significantly reduced by FG derivatives, which offer a more direct and straightforward control over material's characteristics.

Carboxylic acids functionalized graphenes can be implemented as carbocatalysts, i.e. a heterogeneous carbon-based materials where the

* Corresponding author. Department of Chemical Science and INSTM Unit, University of Padova, Via F. Marzolo 1, 35131, Padova, Italy.

E-mail address: stefano.agnoli@unipd.it (S. Agnoli).

carbon atoms or specific active sites enable an efficient chemical conversion [20,21]. In this context, it is quite intriguing to investigate whether these systems can exhibit a catalytic activity similar to that of natural enzymes [22]. This is important not only because it can significantly impact a wide range of reactions and chemical processes [23,24], but also due to its relevance in various interdisciplinary fields such as nanomedicine, toxicology, bioelectrochemistry, sensors, where the interaction of carbon nanomaterials with biological systems plays a crucial role. In this work, optimizing a sustainable synthesis route, we prepared in high yield a graphenic material rich in carboxylic acids, called Graphene Acetic Acid (GAA). Previously, a derivative of fluorographite synthesized using a malonic ester was already reported in the literature, but using a less sustainable protocols based on 1,2-dichlorobenzene as solvent and an organic base, and reaching a lower final functionalization degree [25]. As a case study, we investigated a reaction involving reactive oxygen species (ROS), specifically the reduction of hydrogen peroxide to water, a process that is typically catalyzed by the enzyme peroxidase in biological systems.

Several natural enzymes utilize high-valency iron species for a wide range of reactions, therefore artificial mimics, called nanozymes, which exploit the chemistry of iron [26] have been largely studied in the past. On the contrary, the literature regarding catalase or peroxidase activity in metal-free catalysts is relatively limited [23]. To evaluate the catalytic properties of GAA in advanced oxidation reactions within a broader context, we investigated the oxidation of sulfides to sulfoxides. This is particularly relevant in medicinal chemistry, where sulfoxides are important functional groups extensively used in synthetic drugs, such as modafinil [27] or sulindac [28]. Most of the syntheses used at present start from sulfides and use various oxidants, such as m-CPBA [29] or Oxone [30], whereas the utilization of H₂O₂ would be highly preferable from a Green Chemistry perspective [31].

In both reactions, we found that GAA exhibits outstanding catalytic activity, surpassing the performance of previously reported carbon nanomaterials and even of most metal catalysts. This remarkable efficiency underscores the still untapped potential of GAA for chemical conversion applications.

2. Experimental

2.1. Synthesis of GAA

50 mL of anisole is added in a three neck round bottom flask under an inert atmosphere, following three vacuum/nitrogen cycles. An amount of 333 mg of FG is added to the flask and the resulting suspension is sonicated for 4 h. In a 200 ml beaker, 26 g of potassium carbonate and 12 mL of diethylmalonate are allowed to react in an ice bath in 50 mL of anisole for 1 h under magnetic stirring. The second solution is added to the first suspension, heated and left to react at 130 °C for 24 h. The resulting solution is filtered through a PTFE membrane and then washed with 100 ml of dimethyl formamide (DMF), 100 × 2 mL of acetone and then washed with 100 × 3 ml of water on a polycarbonate (PC) membrane.

The resulting product is dispersed in 100 ml of water in a round bottom flask, adjusted to pH ~3 with H₂SO₄ and sonicated for 1 h. The solution is then refluxed for 24 h. Afterward it is filtrated through a PC membrane and then washed with water until a neutral pH is reached. Finally, In the end the compound is washed with 100 × 3 mL of acetone and allowed to dry.

2.2. Peroxidase-like activity

The peroxidase like activity assays of GAA were performed using 3,3',5,5'-tetramethylbenzidine (TMB) as the substrate in the presence of H₂O₂ either in 0.1 M acetic acid-sodium acetate buffer solution (pH = 4) or in a phosphate buffer (pH = 7).

To monitor the kinetics of the reaction, the absorbance at 652 nm of

the solution containing the oxidation products (3,3',5,5'-tetramethylbenzidine diimine, oxTMB) was measured as over time by a Cary 500 UV-Vis spectrophotometer. Each activity data point represents the average of three replicates. Experiments conducted in the absence either of H₂O₂ or GAA showed no relevant activity. In order to extract the kinetic data, different sets of experiments were performed both by varying the H₂O₂ concentration (up to 0.5 M) for a fixed amount of TMB and vice versa (up to 10⁻⁴ M). The reaction rate was determined by fitting the initial linear portion of the curve describing the evolution of the concentration of the oxTMB as a function of time. By plotting the reaction rate vs the substrate concentration (either H₂O₂ or TMB) a typical Michaelis-Menten saturation curve was observed:

$$V = \frac{V_{max}[S]}{K_M + [S]}$$

allowing to determine by a simple fitting procedure the values of V_{max} and K_M. To compare the kinetics at different concentrations, we used the Lineweaver-Burk plot based on the following equation:

$$\frac{1}{V} = \frac{K_M}{V_{max}[S]} + \frac{1}{V_{max}}$$

2.3. Sulfides oxidation

In a standard test, 1 mg of GAA is placed in a 20 mL vial. Then a volume of 300 μL of 30 % hydrogen peroxide is added. The dispersion is sonicated for 10 min while keeping the vial sealed. At this point, 0.117 mL of thioanisole is added. The reaction occurs at room temperature under 200 rpm magnetic stirring. After a specific time, the crude product is recovered using 1 mL of THF. Subsequently, the solid material is separated by centrifugation (6500 rpm for 3 min). The resulting solution is then dissolved in deuterated chloroform and analyzed by NMR. Conversion calculated as $\frac{I_{sulphone} + I_{sulphoxide}}{I_{total}}$ and selectivity as $\frac{I_{sulphone}}{I_{sulphone} + I_{sulphoxide}}$, where "I" is the integral intensity of the NMR signal centered at 2.46 ppm for thioanisole, 2.67 ppm for sulfoxide and 3.04 ppm for sulfone.

2.4. EPR measurements

Spin-trapping EPR measurements were performed using an ELEXSYS Bruker spectrometer operating at X-band, equipped with a CF935 cryostat and a Flexline MD5 dielectric cavity. The measurements were conducted in quartz tubes open to air. The concentrations used were: 2 mL of 5 mg/mL of GAA in phosphate buffer 1 M, 150 μL of 25 mg/L 5,5-Dimethyl-1-pyrroline N-oxide (DMPO) in EtOH, 5 μL H₂O₂.

The temperature-dependent cw-EPR measurements were performed using an X-band RADIOPAN SX spectrometer with a TM110 cylindrical cavity. Oxford ESR900 continuous flow cryostat enabled measurements over the temperature range of 4.2–300 K.

2.5. Physicochemical characterization

The surface chemical characterization of the materials was performed using X-ray photoemission spectroscopy (XPS) in a custom-made UHV system operating at a base pressure of 10⁻¹⁰ mbar, equipped with an Omicron EA125 electron analyzer and an Omicron DAR 400 X-ray source with a dual Al-Mg anode. Core level photoemission spectra (C 1s, N 1s, O 1s, F 1s) were collected at room temperature (rt) with a non-monochromatic Al Kα X-ray source (1486.6 eV) and using an energy step of 0.1 eV, 0.5 s of integration time, and 20 eV of pass energy. The samples were suspended in 2-propanol and drop-cast on an Cu metal support. Samples were performed on a High Resolution Transmission Electron Microscope (HRTEM) Titan G2 60–300 (FEI) with Image corrector on accelerating voltage of 80 kV. Images were taken with BM UltraScan CCD camera (Gatan). Energy Dispersive Spectrometry (EDS) was performed in Scanning TEM (STEM) mode by Super-X system with

four silicon drift detectors (Bruker). Solid state Fourier Transformed Infrared (FT-IR, KBr disk technique) absorption spectra were recorded with a Nicolet Nexus FT-IR spectrometer. ζ -potential measurements were carried on Malvern Panalytical Zetasizer Nano ZS90 using 0.1 mg/mL suspensions of GAA in water. The pH was adjusted between 3 and 11 using NaOH and HCl. XRD was recorded using a Panalytical AERIS Research instrumentation, using Cu K α radiation ($\lambda = 0.15406$ nm) at 30 kV and 15 mA. Nuclear Magnetic Resonance (NMR) spectra were recorded on a Bruker Avance 300 MHz spectrometer (300.1 MHz for ^1H , 298 K); chemical shifts (δ) are reported in parts per million (ppm) relative to the residual solvent signals and coupling constants (J) are expressed in Hz. The solid-state ^{13}C MAS spectrum was acquired on a Jeol ECZR 600 spectrometer (150.9 MHz for ^{13}C). The powder sample was packed into a cylindrical zirconia rotor with a 3.2 mm outer diameter (60 μL volume) and spun at 20 kHz. The spectrum was acquired at room temperature and an optimized recycle delay of 20 s was used for 450 scans. The ^{13}C chemical shift scale was calibrated through the methylenic signal of external standard α -glycine (at 43.7 ppm).

3. Results and discussion

3.1. GAA synthesis and characterization

For the preparation of GAA (see Scheme 1), we adopted a strategy based on the nucleophilic substitution of the fluorine atoms of FG that was previously employed for the synthesis of graphene acid [11]. However, in this case we substituted the highly toxic cyanide ions with diethylmalonate anions, produced *in situ* by the reaction of a strong base (i.e. potassium carbonate) with diethylmalonate. As seen in numerous examples in the literature, FG is particularly susceptible to nucleophilic attack on radical point defects generated by fluorine elimination, which leads to the covalent attachment of the nucleophile and consequently to a bond rearrangements in the carbon backbone resulting in the formation of vacancies and new radical defects [32–36]. The methylene units can attach either to C sp^2 atoms next to edges or vacancies or to C sp^3 atoms deriving from the original backbone of FG. A subsequent acid treatment at moderate temperature (~ 100 °C) induces the hydrolysis of the esters and decarboxylation of the diacid groups [37], leading to the formation of a novel graphenic material with $-\text{CH}_2\text{-COOH}$ pendants directly installed on the basal plane. Initially, the synthesis was carried out in DMF, but to identify a more environmentally friendly reaction medium, various solvents were evaluated. While benzylic alcohol solubilized all reactants, some of the benzylic functionalities were incorporated into the graphene backbone. The use of ethylene glycol led in a lower functionalization because of an undesired solvent polymerization with diethylmalonate. Ultimately, anisole was identified as the optimal solvent, producing the same material as DMF. The reaction was also tested using neat diethylmalonate, yielding the desired results, however, the large quantity of diethylmalonate required makes anisole a more environmentally friendly alternative.

To confirm the successful preparation of GAA, the resulting material was characterized by several spectroscopic techniques. In the IR spectra (Fig. 1a), FG shows strong absorption peaks at ~ 1200 cm^{-1} associated with C–F vibrations, whereas the final product exhibits broad C=C peaks at 1582 cm^{-1} , attributed to the stretching of the aromatic structures typical of graphenic materials [38], as well as characteristic carboxylic acids signals at 1716 cm^{-1} (Fig. S1). Furthermore, signals at 2851 and 2915 cm^{-1} corresponding to C–H stretching modes, are

observed. To confirm that the carboxylic acid signals were not related to other carbonyls derivatives, the material was first exposed to a base and then to an acid, observing the disappearance and reappearance of the signal related to carboxyl stretching vibrations. As a further confirmation, after the basic treatment we also observed the carboxylate signals at ~ 1430 cm^{-1} (Fig. 1a).

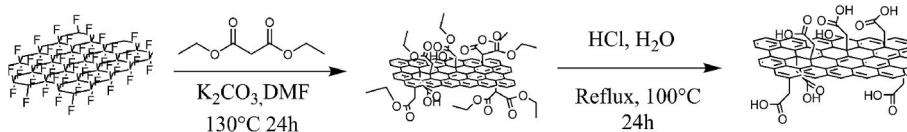
XPS data show (Figs. S3 and S3 in the Supplementary Information) the presence of the core levels of C 1s and O 1s, while the F 1s photoemission peak is barely detectable, indicating a residual concentration of fluorine atoms below 1 % at/at. Moreover, the C 1s photoemission line does not show any appreciable component related to C–F species at 290 eV (Fig. 1b). The deconvolution of the C 1s spectrum into chemically shifted components (Fig. 1b) indicates a sp^2 carbon content of 60 at. %, proving the formation of a graphenic network, a sp^3 content of 18 at. % likely associated with the methylene units of the acetic groups, 12 at. % of oxygen-related species, likely alcohols and 10 at. % of carboxylic acids (see Table S1 in the Supplementary Information).

XRD analysis (Fig. S4) shows the typical diffraction features of graphene-based materials. According to the literature [39], standard interlayer distances of 0.9 nm and 0.4 nm correspond to 2θ values of 12.5° and 23.8° , respectively. These signals are typically associated with diffraction from the (002) planes of graphene oxide (GO) and reduced graphene oxide (rGO), respectively. Additionally, we can detect a large peak at $2\theta = 43^\circ$, which is commonly attributed for both GO and rGO to the internal order within the graphene layer i.e. to the (100) reflections [40].

To further characterize the nature and amount of functional groups on the material, we acquired solid-state ^{13}C NMR measurements. The ^{13}C -MAS spectrum reported in Fig. 1c indicates the presence of well resolved peaks, in particular two distinct components in the low ppm region corresponding to saturate carbons and the feature at 162 ppm, accounting for 9.9 % of the total intensity, which can be associated with carboxyl groups [41], in excellent agreement with the XPS data. Moreover, the peak at 11.2 ppm (6.2 % of the total intensity) indicates defective carbon lacking conjugation with graphenic plane, while the signal at 27.2 ppm can be attributed to the methylene units between the graphenic plane and carboxylic acid groups, and finally the peak corresponding to carbons with alcohol functionalities is observed at 60 ppm.

Given the interest of this material, for redox reactions we used EPR spectroscopy to identify and quantify the possible presence of free electrons and their localization within the carbon backbone.

Continuous-wave (cw) EPR measurements on GAA powder in the 4–300 K range confirm the presence of unpaired electrons. The structureless line (see inset in Fig. 1d, and Fig. S5 and Table S2) has been deconvoluted into two Lorentzian components with nearly the same g-value, but rather different linewidth: 0.16 (component “1”) and 0.48 mT (component “2”), and relative intensities 1:2 respectively. These components are representative of the paramagnetic dominant species. The spin concentration obtained by double integration of the line at room temperature is $5 \cdot 10^{18}$ spin/g by comparison with a Mn(II) standard sample [42]. The presence of structureless Lorentzian components indicates a strong spin exchange interaction between paramagnetic centers [43,44]. Further information on the nature of the centers was obtained by studying the temperature dependence of the intensity. Fig. 1d reports the inverse intensity of the two components as a function of the temperature: component “1” is rather temperature independent in the range 50–300 K, and it shows a small decrease below this range,



Scheme 1. Synthesis protocol of GAA starting from FG.

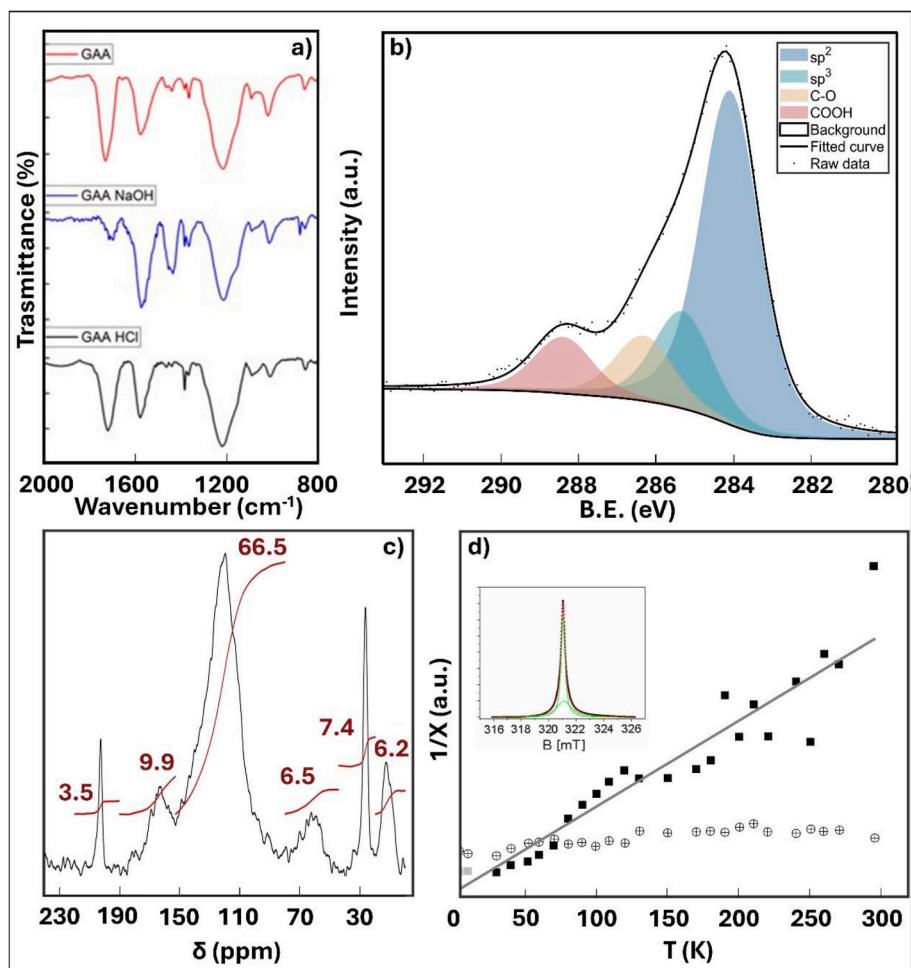


Fig. 1. a) IR spectra of as prepared GAA (red), after basic treatment (blue) and subsequential acid treatment (black) b) C 1s XPS spectra of GAA c) ^{13}C MAS NMR spectrum of GAA sample recorded at 150.9 MHz with the integration of the relevant peaks for quantification. d) inverse of the EPR intensity as function of the temperature for component 1 (circles) and component 2 (squares) together with its linear fit (grey line); the experimental points at the lowest temperatures of component 2 are probably affected by saturation, therefore they are reported in grey. In the inset the cw-EPR spectrum of GAA at room temperature (integration of the cw-EPR spectrum) together with the fitting as sum of two Lorentzian components (green lines). (For interpretation of the references to color in this figure legend, the reader is referred to the Web version of this article.)

while component “2” has a typical Curie-type linear trend with an intercept on the abscissa axis at T nearly 0 K.

Based on these data, we assign component 1, having a mild temperature dependance, to partially delocalized electrons located on the edge of the material or to conductive electrons belonging to the same bath [35,36]. Because of the high g -value ($g = 2.0038$ at 50 K), we are in favor to attribute the signal to edge states. Edge states are characterized by the presence of unpaired electrons localized on the p -orbital of C atoms at the boundaries of π -orbitals. Component 2, having a pure paramagnetic Curie-type behavior, is attributed to unpaired electrons in defective sites, with electrons localized in small π -regions on the graphene plane (unpaired electrons on limitedly extended π -orbitals or dangling bonds). Strong exchange interactions between conduction electrons and localized paramagnetic defects have been observed in graphenic-like material and on graphene oxide, and are characteristic of nano-sized materials [45,46], having edge states or defects near electrons in extended π orbitals. Paramagnetic centers are known to be present in the FG [47], therefore we expect that some paramagnetic defectivity remains also after the synthesis protocol.

Non-interacting electrons localized in defects have been detected by pulse methods, which act as a T_2 -filter able to select only slow relaxing species [48]. Indeed (see Fig. S6) the spectrum is composed of two major components with Gaussian line shape, which indicates an unresolved

interaction of the unpaired electrons with a variety of paramagnetic nuclei (likely protons). Notably, the presence and the nature of these radicals are directly related to the catalytic activity of graphene-based materials [8,49].

The acid chemistry of GAA is highlighted from zeta potential analysis at different pH (Fig. S7). While there is almost no response at pH below the pK_a of phenylacetic acid (~ 5.2), an increase in pH leads to the formation of a negative zeta potential value between -50 mV and -30 mV, indicating a very stable dispersion.

TEM images (Fig. S8) show nanosheets with a lateral dimension of hundreds of nanometers, while in general graphene oxide flakes range from few micrometers up to hundreds of nanometers [50]. GAA nanosheets are highly transparent, characterized by slightly jagged edges, and are very stable under the electron beam. The formation of aggregates made by a few stacked flakes is common, and strongly dependent on the preparation of the TEM grid. Lastly from TGA analysis (Fig. S9) the material remains very stable until 200 °C, whereas at 317 °C a 30 % weight loss can be correlated to the loss of carboxylic functionalities [51]. A last weight loss, which accounts for 7.5 % of the mass, is visible at 561 °C and can be associated with defective carbon atoms and oxygenated species, evolving CO and CO_2 [52,53]. and after that, the material remains stable until 800 °C, suggesting that only a graphenic backbone is left.

In conclusion, the experimental data confirms that the GAA comprises highly dispersible graphenic layers, with a lateral dimension typical of several hundred nanometers, which are selectively decorated by acetic acid groups (about 10 %). The defluorination and nucleophilic reactions involved in the synthesis protocol are very effective at eliminating the fluorine atoms, but induce a certain number of structural defects (sp^3 carbon), including a significant amount of trapped electrons.

3.2. Catalytic activity

3.2.1. Biomimetic peroxidase activity

To evaluate the catalytic activity of GAA as a peroxidase mimic, we used a well-established colorimetric test based on the oxidation of TMB [54]. This molecule can be oxidized by H_2O_2 to 3,3',5,5'-tetramethylbenzidine diimine (oxTMB) producing a deep blue solution, therefore the kinetics of the reaction can be easily followed by monitoring the intensity of the oxTMB adsorption band, centered at $\lambda = 652$ nm, over time.

As reported in Fig. 2a and b, the plot of the reaction rate versus the concentration of catalytic substrate, either TMB or H_2O_2 , returns a rectangular hyperbola, which is typical of the Michaelis-Menten kinetics of enzyme catalyzed reactions. By fitting the experimental data to the Michaelis-Menten equation through non-linear regression methods, we could extract K_m and V_{max} , i.e. the affinity of the catalyst for the substrate and the limiting rate of the reaction. The same apparent

kinetic parameters were also obtained by the analysis of Lineweaver–Burk plot (or double reciprocal plot), as reported in Fig. 2c.

Table 1 reports the values of the catalytic figures of merit of GAA as well as those of related benchmarks found in the literature in similar experimental conditions. Clearly, GAA outperforms the best previously reported graphene-based catalyst, a highly carboxylated form of graphene oxide [23], as indicated by the higher values of V_{max} , whereas the k_m values are comparable. Notably, GAA exhibits superior catalytic activity compared to other peroxidase mimics based on transition metals [55–57]. The comparison between the catalytic activity at pH = 4 and pH = 7 (reported in Fig. S10) reveals that, although V_{max} is higher at pH = 4, as expected for TMB oxidation, the k_m value suggests a better substrate affinity at pH = 7, likely due to the improved material dispersion. Quite interestingly, the double reciprocal plot (Fig. 2c) shows that the kinetic profiles of TMB oxidation carried out at different H_2O_2 concentration produce parallel curves, which is the fingerprint of a ping-pong mechanism, as observed for HRP [58] and other selected nanozymes [54]. This means that GAA binds and reacts with a catalytic substrate, releases the first product, and then the intermediate form of the catalyst binds and reacts with the second substrate.

To further understand the nature of the activity of GAA in this reaction, an EPR spin trapping experiment was performed (Fig. S11 and Table S3). As a matter of fact, the identification of the ping pong mechanism suggests that GAA could act as a redox mediator, forming a reversible intermediate active state during reaction conditions. Indeed,

Table 1

Michaelis Menten parameters comparison.

Catalyst	Substrate	K_m (mM)	V_{max} (nM/s)
GAA	TMB (50 mM H_2O_2)	0.0845	1437
	H_2O_2 (0.8 mM TMB)	27	32100
GO-COOH in AM 2008 [23]	TMB (50 mM H_2O_2)	0.023	34.5
	H_2O_2 (0.8 mM TMB)	3.99	38.5
Horseradish peroxidase (HRP)	TMB	0.275	12.4
	H_2O_2	0.214	24.6
Fe_3O_4 MNPs [55]	TMB	0.098	34.4
	H_2O_2	154	97.8
$Co_3(PO_4)_2$ [57]	TMB	0.136	8
	H_2O_2	0.073	12
PN-Ceria [56]	TMB	0.147	6200
	H_2O_2	293	3800

the ability of oxidized graphene derivatives and carbon materials to act as redox mediators has been well documented by several works [54,59]. To shed some light on the possible mechanism we introduced DMPO in the reaction environment with the idea of identifying possible radical intermediates generated by the main oxidant, H_2O_2 .

While in the absence of GAA the only visible signals are from decomposed DMPO [60] and ethanol [61], when the GAA is added, a new set of signals arises, with coupling constant comparable to that of DMPO trapped in benzoic acid [62], indicating the formation of a radical possibly deriving from the peroxyacid formed by the reaction of a carboxylic group with H_2O_2 . These data therefore likely suggest that the intermediate form of the catalyst is a surface peracid that in the second step of the reaction cycle reacts with the TMB to give the final oxidation product. We also mentioned that in presence of O_2 , but without H_2O_2 the oxidation of TMB does not proceed in a significant amount, and no superoxide species has been detected, ruling out other possible reaction mechanisms involving other ROS, which were previously reported in the literature for carbon nanomaterials [8].

3.2.2. Sulfide oxidation

Given the excellent performance of GAA in the activation of H_2O_2 for the oxidation of organic compounds, we investigated the potential of this catalyst for more challenging reactions that require high selectivity and are extremely relevant for fine chemical synthesis.

As a case study we investigated the oxidation of organic sulfides to sulfoxides using green chemistry protocols i.e. using H_2O_2 as oxidizing agent, at room temperature and without the use of additional solvents, to reduce the chemical waste. NMR spectroscopy was used to identify the reaction products and quantify the yield and selectivity.

The results of the oxidation of thioanisole to sulfoxide are shown in Fig. 3. GAA proved to be an outstanding catalyst in the oxidation of thioanisole affording the corresponding sulfoxide in a short time (200 min for complete conversion) without the addition of any solvent and at room temperature. No traces of sulfones, i.e. the total oxidation product, or other compounds were detected. Moreover, after the catalytic test, the catalyst can be easily recovered through filtration and reused for further catalytic cycles without changes in the selectivity or

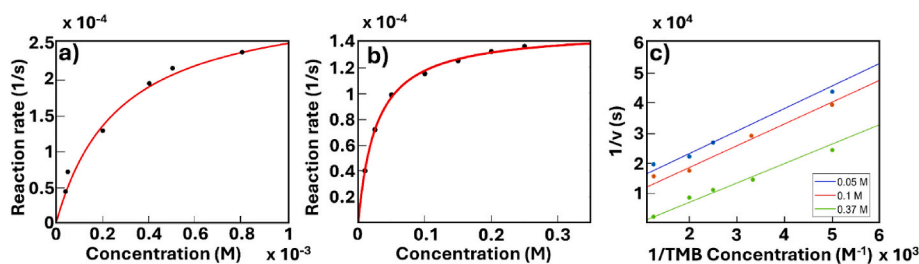


Fig. 2. a) Michaelis Menten behavior changing TMB concentration b) Michaelis Menten behavior changing H_2O_2 concentration c) double reciprocal plot (Lineweaver–Burk) at different H_2O_2 concentration.

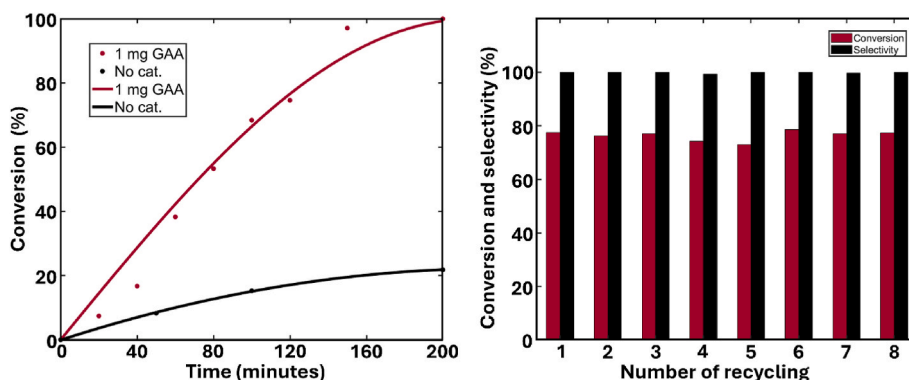
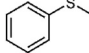
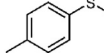
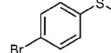
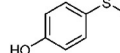
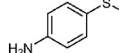
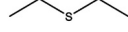


Fig. 3. a) Oxidation kinetic of thioanisole in presence and absence of catalyst b) Conversion and selectivity at 120 min (around 80 % yield) for different recycling tests.

productivity. The medicinal compound targets of this type of oxidation present a variety of functional groups, therefore the catalyst must be selective not only towards the oxidation to sulfoxide, but must also prevent the oxidation of other functional groups potentially present on the catalytic substrate. To confirm this high selectivity and the tolerance to the presence of different chemical moieties, we attempted the conversion of different compounds, and the results are shown in Table 2. In all cases, the only oxidation process is the oxidation of sulfide to sulfoxide. In the case of both 4-methylthioanisole and 4-bromothioanisole the conversion decreases significantly (59 % and 44 %, respectively), while for 4-(Methylmercapto)phenol and 4-(Methylmercapto)aniline we observe an opposite effect, suggesting that rather than electronic effects, the presence of protic groups plays a major role on the reactivity. When a non-aromatic substrate, such as diethylsulfide, is considered, the conversion is higher compared with thioanisole (99 %), while keeping a good selectivity (96 %). In the literature, other graphene-based materials have been already used for sulfide oxidation, however in general it is reported that modified GO preferentially catalyzes the conversion toward sulphones. Previously, Bielawski et al. showed that graphene oxide exhibited a good activity and similar selectivity for this same reaction, but in that case, the loading of graphene oxide was 300 % wt. higher compared to the catalytic substrate, raising some doubts about the genuinely catalytic nature of the reaction [63]. On the other hand, Abdi et al. [64] proposed a carboxyl-decorated graphene oxide that was selective towards the total oxidation to sulfone. The authors suggested a concerted mechanism, in which two different peroxy acid groups attached on vicinal positions of the graphene edge, enable the direct oxidation from sulfide directly to sulphone. On the contrary, GAA despite the presence of similar functional groups on the surface, selectively promotes the partial oxidation to sulfoxide. This can be explained by the subtle differences in the structures of the two materials. In GAA the carboxylic acid pendants are more homogeneously dispersed on both sides of the whole basal plane, as also seen in other syntheses from FG [65] whereas on GO derived materials the carboxyl groups are preferentially concentrated on the edges, making possible a synergistic interaction by multiple COOH species on the same molecule, eventually leading to the total oxidations. On both materials however, we can hypothesize that the active species are indeed short-living peroxy acids [66], which are formed by the reaction with H_2O_2 , as we have documented in the previously reported EPR spin trapping experiments.

Table 2
Conversion after 90 min and selectivity toward sulfoxide of different catalytic substrates.

						
Conversion (%)	65	59	44	98	99	99
Selectivity for Sulfoxide (%)	100	98	100	100	93	96

4. Conclusion

A novel, easy, and sustainable synthesis protocol based on the chemistry of FG has been developed for the scalable production of GAA. As demonstrated by the combination of several characterization techniques including XPS, FT-IR, solid state ^{13}C NMR, and EPR spectroscopies, TGA, TEM, this material consists of graphene nanosheets of a few hundred nanometers characterized by a relatively dense and very selective functionalization of the basal plane with acetic acid pendants (about 10 %). Despite its close analogy to Graphene Oxide, GAA, however is highly conductive [16] and characterized by the presence of a large amount of trapped electrons (5×10^{18} per gram), making it quite appealing as a potential catalyst for redox reactions.

This hypothesis was tested by investigating the catalytic properties of GAA in advanced catalytic oxidations involving hydrogen peroxide, a key reactant for Green Chemistry reactions and a widespread ROS. GAA demonstrated to be an outstanding catalyst as peroxidase mimic, showing a clear Michaelis-Menten behavior. Through the analysis of the catalytic tests, we could ascertain a ping-pong mechanism and determine a limiting rate ($V_{max} = 32100$ nM/s) surpassing previously reported carbon materials. Similar excellent properties were also documented in the selective partial oxidation of sulfide to sulfoxide. Interestingly, EPR trapping experiments with DMPO support the idea that in both reactions a key role is played by peroxyacid radicals, which are formed *in situ* by the reaction of GAA with H_2O_2 .

Overall, this work depicts a consistent scenario where GAA, given its unprecedented physicochemical properties, can be used as a general catalytic platform for a variety of reactions. The presence of sp^2 domains and hydrophilic pendants can be exploited to adjust precisely its affinity towards specific catalytic substrates. Moreover, the presence of acid groups makes it an appealing solid acid, while its high electron conductivity and intrinsic redox chemistry can be easily exploited in oxidation and electrochemical reactions. Furthermore, all these strategies can be combined to produce synergistic effects, enabling complex cascade and tandem processes, which are key objectives in Green Chemistry.

CRediT authorship contribution statement

Biagio Di Vizio: Writing – review & editing, Writing – original draft,

Investigation, Formal analysis, Data curation. **Giorgio Lazzari**: Writing – review & editing, Investigation, Formal analysis. **Roman Strzelczyk**: Writing – review & editing, Investigation, Formal analysis, Data curation. **Giacomo De Crescenzo**: Writing – review & editing, Investigation, Formal analysis, Data curation. **Antonio Barbon**: Writing – review & editing, Investigation, Formal analysis, Data curation. **Claudio Garino**: Writing – review & editing, Investigation, Formal analysis, Data curation. **Roberto Gobetto**: Writing – review & editing, Formal analysis, Conceptualization. **Stefano Agnoli**: Writing – review & editing, Supervision, Resources, Methodology, Funding acquisition, Conceptualization.

Declaration of competing interest

The authors declare the following financial interests/personal relationships which may be considered as potential competing interests: Stefano Agnoli reports financial support was provided by Ministry of University and research of Italy. If there are other authors, they declare that they have no known competing financial interests or personal relationships that could have appeared to influence the work reported in this paper.

Acknowledgements

This work was partially supported by the following projects: project C2 chemical complexity (CUP: C93C22009260001), under the MUR program “Dipartimenti di Eccellenza 2023–2027 and by the project #01BIRD2022-UNIPD (MUSYCA) funded by the University of Padova.

Appendix A. Supplementary data

Supplementary data to this article can be found online at <https://doi.org/10.1016/j.carbon.2024.119856>.

References

- [1] K.S. Novoselov, A.K. Geim, S.V. Morozov, D. Jiang, Y. Zhang, S.V. Dubonos, I. V. Grigorieva, A.A. Firsov, Electric field effect in atomically thin carbon films, *Science* 306 (2004) 666–669, <https://doi.org/10.1126/SCIENCE.1102896>.
- [2] V. Georgakilas, J.A. Perman, J. Tucek, R. Zboril, Broad family of carbon nanoallotropes: classification, chemistry, and applications of fullerenes, carbon dots, nanotubes, graphene, nanodiamonds, and combined superstructures, *Chem. Rev.* 115 (2015) 4744–4822, <https://doi.org/10.1021/cr500304f>.
- [3] A.K. Geim, Random walk to graphene, *Int. J. Mod. Phys. B* 25 (2011) 4055–4080, <https://doi.org/10.1142/S0217979211059097>.
- [4] M. Blanco, S. Agnoli, G. Granozzi, Graphene acid: a versatile 2D platform for catalysis, *Isr. J. Chem.* 62 (2022) e202100118, <https://doi.org/10.1002/ijch.202100118>.
- [5] J. Deng, S. Fang, Y. Fang, Q. Hao, L. Wang, Y.H. Hu, Multiple roles of graphene in electrocatalysts for metal-air batteries, *Catal. Today* (2022), <https://doi.org/10.1016/J.CATTOD.2022.01.003>.
- [6] J. Han, I. Johnson, M. Chen, 3D continuously porous graphene for energy applications, *Adv. Mater.* 34 (2022) 2108750, <https://doi.org/10.1002/adma.202108750>.
- [7] M. Lunardon, J. Ran, D. Mosconi, C. Marega, Z. Wang, H. Xia, S. Agnoli, G. Granozzi, Hybrid transition metal dichalcogenide/graphene microspheres for hydrogen evolution reaction, *Nanomaterials* 10 (2020) 2376, <https://doi.org/10.3390/NANO10122376>, 2376 10 (2020).
- [8] C. Su, M. Acik, K. Takai, J. Lu, S.J. Hao, Y. Zheng, P. Wu, Q. Bao, T. Enoki, Y. J. Chabal, K.P. Loh, Probing the catalytic activity of porous graphene oxide and the origin of this behaviour, *Nat. Commun.* 31 3 (2012) 1–9, <https://doi.org/10.1038/ncomms2315> (2012).
- [9] L. Wang, Z. Sofer, M. Pumera, Will any crap we put into graphene increase its electrocatalytic effect? *ACS Nano* 14 (2020) 21–25, <https://doi.org/10.1021/acsnano.9b00184>.
- [10] M. Pumera, Z. Sofer, Towards stoichiometric analogues of graphene: graphane, fluorographene, graphol, graphene acid and others, *Chem. Soc. Rev.* 46 (2017) 4450–4463, <https://doi.org/10.1039/C7CS00215G>.
- [11] A. Bakandritsos, M. Pykal, P. Błoński, P. Jakubec, D.D. Chronopoulos, K. Poláková, V. Georgakilas, K. Cépe, O. Tomanec, V. Ranc, A.B. Bourlinos, R. Zboril, M. Otyepka, Cyanographene and graphene acid: emerging derivatives enabling high-yield and selective functionalization of graphene, *ACS Nano* 11 (2017) 2982–2991, <https://doi.org/10.1021/acsnano.6b08449>.
- [12] P. Tang, B. Di Vizio, J. Yang, B. Patil, M. Cattelan, S. Agnoli, Fe,Ni-Based metal-organic frameworks embedded in nanoporous nitrogen-doped graphene as a highly efficient electrocatalyst for the oxygen evolution reaction, *Nanomaterials* 14 (2024) 751, <https://doi.org/10.3390/nano14090751>.
- [13] M. Medved, G. Zoppellaro, J. Ugolotti, D. Matochová, P. Lazar, T. Pospíšil, A. Bakandritsos, J. Tucek, R. Zboril, M. Otyepka, Reactivity of fluorographene is triggered by point defects: beyond the perfect 2D world, *Nanoscale* 10 (2018) 4696–4707, <https://doi.org/10.1039/c7nr09426d>.
- [14] M. Blanco, D. Mosconi, M. Otyepka, M. Medved, A. Bakandritsos, S. Agnoli, G. Granozzi, Combined high degree of carboxylation and electronic conduction in graphene acid sets new limits for metal free catalysis in alcohol oxidation, *Chem. Sci.* 10 (2019) 9438–9445, <https://doi.org/10.1039/c9sc02954k>.
- [15] D. Mosconi, M. Blanco, T. Gatti, L. Calvillo, M. Otyepka, A. Bakandritsos, E. Menna, S. Agnoli, G. Granozzi, Arene C–H insertion catalyzed by ferrocene covalently heterogenized on graphene acid, *Carbon N. Y.* 143 (2019) 318–328, <https://doi.org/10.1016/J.CARBON.2018.11.010>.
- [16] R.C. Hensel, B. Di Vizio, V. Montes-García, J. Yang, G.G. Ilie, F. Sedona, M. Sambri, P. Samori, A. Cester, S. Agnoli, S. Casalini, Graphene acetic acid-based hybrid supercapacitor and liquid-gated transistor, <https://doi.org/10.1002/aelm.202300685>, 2024.
- [17] W. Feng, P. Long, Y. Feng, Y. Li, Two-dimensional fluorinated graphene: synthesis, structures, properties and applications, *Adv. Sci.* 3 (2016), <https://doi.org/10.1002/advs.201500413>.
- [18] W.H. Lee, J.W. Suk, H. Chou, J. Lee, Y. Hao, Y. Wu, R. Piner, D. Akinwande, K. S. Kim, R.S. Ruoff, Selective-area fluorination of graphene with fluoropolymer and laser irradiation, *Nano Lett.* 12 (2012) 2374–2378, <https://doi.org/10.1021/nl300346j>.
- [19] R. Ikram, B.M. Jan, W. Ahmad, An overview of industrial scalable production of graphene oxide and analytical approaches for synthesis and characterization, <https://doi.org/10.1016/j.jmrt.2020.08.050>, 2020.
- [20] D.R. Dreyer, C.W. Bielawski, Carbocatalysis: heterogeneous carbons finding utility in synthetic chemistry, *Chem. Sci.* 2 (2011) 1233–1240, <https://doi.org/10.1039/c1sc00035g>.
- [21] C. Su, K.P. Loh, Carbocatalysts: graphene oxide and its derivatives, *Acc. Chem. Res.* 46 (2013) 2275–2285, <https://doi.org/10.1021/ar300118v>.
- [22] S. Jin, C. Wu, Z. Ye, Y. Ying, Designed inorganic nanomaterials for intrinsic peroxidase mimics: a review, *Sensor. Actuator. B Chem.* 283 (2019) 18–34, <https://doi.org/10.1016/J.SNB.2018.10.040>.
- [23] Y. Song, K. Qu, C. Zhao, J. Ren, X. Qu, Graphene oxide: intrinsic peroxidase catalytic activity and its application to glucose detection, *Adv. Mater.* 22 (2010) 2206–2210, <https://doi.org/10.1002/adma.200903783>.
- [24] D.O. Lopez-Cantu, R.B. González-González, E.M. Melchor-Martínez, S.A. H. Martínez, R.G. Araújo, L. Parra-Arroyo, J.E. Sosa-Hernández, R. Parra-Saldívar, H.M.N. Iqbal, Enzyme-mimicking capacities of carbon-dots nanozymes: properties, catalytic mechanism, and applications – a review, *Int. J. Biol. Macromol.* 194 (2022) 676–687, <https://doi.org/10.1016/j.ijbiomac.2021.11.112>.
- [25] A. Bakandritsos, D.D. Chronopoulos, P. Jakubec, M. Pykal, K. Cépe, T. Steriotis, S. Kalytchuk, M. Petr, R. Zboril, M. Otyepka, High-performance supercapacitors based on a zwitterionic network of covalently functionalized graphene with iron tetraaminophthalocyanine, *Adv. Funct. Mater.* 28 (2018), <https://doi.org/10.1002/adfm.201801111>.
- [26] O. Zozulia, L.R. Marshall, I. Kim, E.M. Kohn, I.V. Korendovych, Self-assembling catalytic peptide nanomaterials capable of highly efficient peroxidase activity, *Chem. Eur. J.* 27 (2021) 5388–5392, <https://doi.org/10.1002/chem.202100182>.
- [27] C.A. Czeisler, J.K. Walsh, T. Roth, R.J. Hughes, K.P. Wright, L. Kingsbury, S. Arora, J.R.L. Schwartz, G.E. Niebler, D.F. Dinges, Modafinil for excessive sleepiness associated with shift-work sleep disorder, *N. Engl. J. Med.* 353 (2005) 476–486, <https://doi.org/10.1056/nejmoa041292>.
- [28] R.N. Brogden, R.C. Heel, T.M. Speight, G.S. Avery, Sulindac: a review of its pharmacological properties and therapeutic efficacy in rheumatic diseases, *Drugs* 16 (1978) 97–114, <https://doi.org/10.2165/00003495-197816020-00001>.
- [29] R. Curci, R.A. DiPrete, J.O. Edwards, G. Modena, Experiments bearing on the role of solvent in the oxidation of some organic compounds by peroxy acids, *J. Org. Chem.* 35 (1970) 740–745, <https://doi.org/10.1021/jo00828a044>.
- [30] R.V. Kupwade, S.S. Khot, U.P. Lad, U.V. Desai, P.P. Wadgaonkar, Catalyst-free oxidation of sulfides to sulfoxides and diethylamine catalyzed oxidation of sulfides to sulfones using Oxone as an oxidant, *Res. Chem. Intermed.* 43 (2017) 6875–6888, <https://doi.org/10.1007/s11164-017-3026-0>.
- [31] I. Triandafillidi, D.I. Tzaras, C.G. Kokotos, Green organocatalytic oxidative methods using activated ketones, *ChemCatChem* 10 (2018) 2521–2535, <https://doi.org/10.1002/CCTC.201800013>.
- [32] R. Langer, D. Zaoralová, M. Medved, P. Banáš, P. Błoński, M. Otyepka, Variability of C–F bonds governs the formation of specific structural motifs in fluorinated graphenes, *J. Phys. Chem. C* 123 (2019) 27896–27903, <https://doi.org/10.1021/acs.jpcc.9b07552>.
- [33] M. Medved, G. Zoppellaro, J. Ugolotti, D. Matochová, P. Lazar, T. Pospíšil, A. Bakandritsos, J. Tucek, R. Zboril, M. Otyepka, Reactivity of fluorographene is triggered by point defects: beyond the perfect 2D world, *Nanoscale* 10 (2018) 4696–4707, <https://doi.org/10.1039/c7nr09426d>.
- [34] D. Zaoralova, V. Hrubý, V. Šedajová, R. Mach, V. Kupka, J. Ugolotti, A. Bakandritsos, M. Medved, M. Otyepka, Tunable synthesis of nitrogen doped graphene from fluorographene under mild conditions, *ACS Sustain. Chem. Eng.* 8 (2020) 4764–4772, <https://doi.org/10.1021/acssuschemeng.9b07161>.
- [35] D.D. Chronopoulos, A. Bakandritsos, M. Pykal, R. Zboril, M. Otyepka, Chemistry, properties, and applications of fluorographene, *Appl. Mater. Today* 9 (2017) 60–70, <https://doi.org/10.1016/j.apmt.2017.05.004>.

- [36] C. Bosch-Navarro, M. Walker, N.R. Wilson, J.P. Rourke, Covalent modification of exfoliated fluorographite with nitrogen functionalities, *J. Mater. Chem. C* 3 (2015) 7627–7631, <https://doi.org/10.1039/C5TC01633A>.
- [37] B.R. Brown, The mechanism of thermal decarboxylation, *Q. Rev. Chem. Soc.* 5 (1951) 131–146, <https://doi.org/10.1039/QR9510500131>.
- [38] C. Zhang, D.M. Dabbs, L.M. Liu, I.A. Aksay, R. Car, A. Selloni, Combined effects of functional groups, lattice defects, and edges in the infrared spectra of graphene oxide, *J. Phys. Chem. C* 119 (2015) 18167–18176, <https://doi.org/10.1021/acs.jpcc.5b02727>.
- [39] N. Sirotkin, V. Korolev, Synthesis and characteristics of graphene-graphene oxide material obtained by an underwater impulse direct current discharge, <https://doi.org/10.21203/rs.3.rs-2607964/v1>, 2023.
- [40] M.P. Lavin-Lopez, A. Paton-Carrero, L. Sanchez-Silva, J.L. Valverde, A. Romero, Influence of the reduction strategy in the synthesis of reduced graphene oxide, *Adv. Powder Technol.* 28 (2017) 3195–3203, <https://doi.org/10.1016/j.apt.2017.09.032>.
- [41] T. Azais, G. Hartmeyer, S. Quignard, G. Laurent, F. Babonneau, Solution state NMR techniques applied to solid state samples: characterization of benzoic acid confined in MCM-41, *J. Phys. Chem. C* 114 (2010) 8884–8891, <https://doi.org/10.1021/jp910622m>.
- [42] F. Tampieri, M. Tommasini, S. Agnoli, M. Favaro, A. Barbon, N-doped graphene oxide nanoparticles studied by EPR, *Appl. Magn. Reson.* 51 (2020) 1481–1495, <https://doi.org/10.1007/s00723-020-01276-0>.
- [43] A. Barbon, EPR spectroscopy in the study of 2D graphene-based nanomaterials and nanographites, in: *Electron Paramagn. Reson.*, The Royal Society of Chemistry, 2018, pp. 38–65, <https://doi.org/10.1039/9781788013888-00038>.
- [44] M.A. Augustyniak-Jabłokow, K. Tadzysak, M. Maćkowiak, S. Lijewski, ESR study of spin relaxation in graphene, *Chem. Phys. Lett.* 557 (2013) 118–122, <https://doi.org/10.1016/j.cplett.2012.12.018>.
- [45] A. Barbon, M. Brustolon, An EPR study on nanographites, *Appl. Magn. Reson.* 42 (2012) 197–210, <https://doi.org/10.1007/s00723-011-0285-6>.
- [46] S.S. Rao, A. Stesmans, Y. Wang, Y. Chen, Direct ESR evidence for magnetic behavior of graphite oxide, *Phys. E Low-Dimensional Syst. Nanostructures* 44 (2012) 1036–1039, <https://doi.org/10.1016/j.physe.2011.07.019>.
- [47] M. Medved, G. Zoppellaro, J. Ugolotti, D. Matochová, P. Lazar, T. Pospíšil, A. Bakandritsos, J. Tuček, R. Zbořil, M. Otyepka, Reactivity of fluorographene is triggered by point defects: beyond the perfect 2D world, *Nanoscale* 10 (2018) 4696–4707, <https://doi.org/10.1039/c7nr09426d>.
- [48] F. Tampieri, A. Barbon, Resolution of EPR signals in graphene-based materials from few layers to nanographites, 36–66, <https://doi.org/10.2174/9781681086934118010005>, 2018.
- [49] Z. Komeily-Nia, J.-Y. Chen, B. Nasri-Nasrabadi, W.-W. Lei, B. Yuan, J. Zhang, L.-T. Qu, A. Gupta, J.-L. Li, The key structural features governing the free radicals and catalytic activity of graphite/graphene oxide, *Phys. Chem. Chem. Phys.* 22 (2020) 3112–3121, <https://doi.org/10.1039/C9CP05488J>.
- [50] X. Lin, X. Shen, Q. Zheng, N. Yousefi, L. Ye, Y.-W. Mai, J.-K. Kim, H. Kong, Fabrication of highly-aligned, conductive, and strong graphene papers using ultralarge graphene oxide sheets the lateral dimensions of precursor GO sheets may play an important role in, <https://doi.org/10.1021/nn303904z>, 2023.
- [51] F. Farivar, P. Lay Yap, R.U. Karunagaran, D. Losic, Thermogravimetric analysis (TGA) of graphene materials: effect of particle size of graphene, graphene oxide and graphite on thermal parameters, *Chimia* 7 (2021) 41, <https://doi.org/10.3390/c7020041>.
- [52] R. Larciprete, S. Fabris, T. Sun, P. Lacovig, A. Baraldi, S. Lizzit, Dual path mechanism in the thermal reduction of graphene oxide, *J. Am. Chem. Soc.* 133 (2011) 17315–17321, https://doi.org/10.1021/JA205168X/SUPPL_FILE/JA205168X_SI_001.PDF.
- [53] Z. Fan, K. Wang, T. Wei, J. Yan, L. Song, B. Shao, An environmentally friendly and efficient route for the reduction of graphene oxide by aluminum powder, *Carbon N. Y.* 48 (2010) 1686–1689, <https://doi.org/10.1016/J.CARBON.2009.12.063>.
- [54] L. Artiglia, S. Agnoli, M.C. Paganini, M. Cattelan, G. Granozzi, TiO₂@CeO_x core-shell nanoparticles as artificial enzymes with peroxidase-like activity, *ACS Appl. Mater. Interfaces* 6 (2014) 20130–20136, <https://doi.org/10.1021/am5057129>.
- [55] L. Gao, J. Zhuang, L. Nie, J. Zhang, Y. Zhang, N. Gu, T. Wang, J. Feng, D. Yang, S. Perrett, X. Yan, Intrinsic peroxidase-like activity of ferromagnetic nanoparticles, *Nat. Nanotechnol.* 2 (2007) 577–583, <https://doi.org/10.1038/nnano.2007.260>.
- [56] Z. Tian, J. Li, Z. Zhang, W. Gao, X. Zhou, Y. Qu, Highly sensitive and robust peroxidase-like activity of porous nanorods of ceria and their application for breast cancer detection, *Biomaterials* 59 (2015) 116–124, <https://doi.org/10.1016/j.biomaterials.2015.04.039>.
- [57] L.-J. Peng, H.-Y. Zhou, C.-Y. Zhang, F.-Q. Yang, Study on the peroxidase-like activity of cobalt phosphate and its application in colorimetric detection of hydrogen peroxide, *Colloids Surfaces A Physicochem. Eng. Asp.* 647 (2022) 129031, <https://doi.org/10.1016/j.colsurfa.2022.129031>.
- [58] D.J. Porter, H.J. Bright, The mechanism of oxidation of nitroalkanes by horseradish peroxidase, *J. Biol. Chem.* 258 (1983) 9913–9924, [https://doi.org/10.1016/S0021-9258\(17\)44585-6](https://doi.org/10.1016/S0021-9258(17)44585-6).
- [59] M. Blanco, B. Nieto-Ortega, A. de Juan, M. Vera-Hidalgo, A. López-Moreno, S. Casado, L.R. González, H. Sawada, J.M. González-Cabret, E.M. Pérez, Positive and negative regulation of carbon nanotube catalysts through encapsulation within macrocycles, *Nat. Commun.* 9 (2018) 2671, <https://doi.org/10.1038/s41467-018-05183-8>.
- [60] F.A. Villamena, J.K. Merle, C.M. Hadad, J.L. Zweier, Superoxide radical anion adduct of 5,5-dimethyl-1-pyrroline N-oxide (DMPO). 2. The thermodynamics of decay and EPR spectral properties, *J. Phys. Chem. A* 109 (2005) 6089–6098, <https://doi.org/10.1021/JP0524330>.
- [61] P.M. Hanna, M.B. Kadiiska, R.P. Mason, Oxygen-derived free-radical and active oxygen complex formation from cobalt(II) chelates in vitro, *Chem. Res. Toxicol.* 5 (1992) 109–115, <https://doi.org/10.1021/tx00025a019>.
- [62] L. Ebersson, M.P. Hartshorn, O. Persson, Inverted spin trapping. Part V. 1,1,1,3,3,3-Hexafluoropropan-2-ol as a solvent for the discrimination between proper and inverted spin trapping, *J. Chem. Soc. Perkin Trans. 2* (1996) 141, <https://doi.org/10.1039/p29960000141>.
- [63] D.R. Dreyer, H.-P. Jia, A.D. Todd, J. Geng, C.W. Bielawski, Graphite oxide: a selective and highly efficient oxidant of thiols and sulfides, *Org. Biomol. Chem.* 9 (2011) 7292, <https://doi.org/10.1039/c1ob06102j>.
- [64] G. Abdi, A. Alizadeh, M.M. Khodaei, Highly carboxyl-decorated graphene oxide sheets as metal-free catalytic system for chemoselective oxidation of sulfides to sulfones, *Mater. Chem. Phys.* 201 (2017) 323–330, <https://doi.org/10.1016/j.matchemphys.2017.08.062>.
- [65] B. Di Vizio, D. Mosconi, M. Blanco, P. Tang, L. Nodari, O. Tomanec, M. Otyepka, S. Pollastri, S. Livraghi, M. Chiesa, G. Granozzi, S. Agnoli, Enhanced selective oxidation of ethylarenes using iron single atom catalysts embedded in Nitrogen-Rich graphene, *Chem. Eng. J.* 499 (2024) 156299, <https://doi.org/10.1016/j.cej.2024.156299>.
- [66] G.R. Schonbaum, S. Lo, Interaction of peroxidases with aromatic peracids and alkyl peroxides, *J. Biol. Chem.* 247 (1972) 3353–3360, [https://doi.org/10.1016/S0021-9258\(19\)45252-6](https://doi.org/10.1016/S0021-9258(19)45252-6).